*Bull. Mater. Sci.*, Vol. 40, No. 5, September 2017, pp. 897–905
DOI 10.1007/s12034-017-1440-y

© Indian Academy of Sciences

# Anisotropic optical properties of ZnS thin films with zigzag structure

**SEYYED ZABIHOLLAH RAHCHAMANI, HAMID REZAGHOLIPOUR DIZAJI* and MOHAMMAD HOSSIEN EHSANI**
Thin Film Laboratory, Faculty of Physics, Semnan University, Semnan 35131-19111, Iran
*Author for correspondence (hrgholipour@semnan.ac.ir)

MS received 5 August 2016; accepted 5 December 2016; published online 18 August 2017

**Abstract.** ZnS sculptured thin films produced by thermal evaporation method using the glancing angle deposition technique at different deposition angles (0, 30, 60, 70 and 80°) are reported. The structural and optical properties of the prepared samples are investigated systematically using X-ray diffraction (XRD) and UV–VIS spectroscopy techniques. The XRD studies show cubic structure for the prepared films and deposition angle dependence of lattice constants, intrinsic stress, tensile stress and dislocation density. The obtained transmittance spectra in the range 380–850 nm for both s- and p-polarized light at normal incidence angle are used to study the s- and p-refractive indices and in-plane birefringence of the ZnS films. The maximum birefringence is evaluated at incident flux angle $\alpha = 70°$. Both the refractive index and packing density of the films decrease with increasing deposition angle, which confirm the structural inhomogeneity and porosity nature of the films.

**Keywords.** Zigzag thin films; glancing angle deposition; microstructure; birefringence.

## 1. Introduction

The glancing angle deposition (GLAD) technique is a well-known method for fabricating and engineering microstructured and nanostructured compound materials. GLAD technique, first reported in 1959 [1], is based on controlling the substrate tilt during growth process. It enables this technique to produce sculptured thin films (STFs) in nanoscale [2–4]. In this process, the self-shadowing effects and limited ad-atom diffusion occur when vapour flux arrives at highly oblique angles to the substrate surface. Hence, highly porous thin films with controlled nanostructures and a variety of columnar film morphologies having anisotropic properties can be grown [5,6]. Figure 1a demonstrates how this technique is used to control the substrate orientation with respect to vapour flux direction, which can be performed with two degrees of freedom ($\alpha$ and $\phi$ angles) using a microcontroller [7]. Here $\alpha$ is the angle of substrate surface normal with respect to the vapour flux direction and $\phi$ is the substrate rotation angle about its normal vector.

For $\phi = 0$, GLAD technique leads to the formation of individual columns facing towards the vapour flux direction. However, for $\phi \neq 0$, some other structures such as inclined columns [8], straight pillars [9], helix [10] and zigzag [11] shapes can be produced.

In the earliest efforts on oblique angle deposition (OAD) [12] and GLAD [13], researchers observed polarization-sensitive properties and anisotropy originating from the microstructure in deposited films. When the incident flow is made oblique, the asymmetry in the vapour distribution produces asymmetric (or anisotropic) shadowing, leading to creation of anisotropic properties in the grown films. The anisotropy produced in OAD films appears in the form of anisotropic film properties such as stress, optical birefringence and dichroism [14], magnetic susceptibility [15] and fluid transport [14].

The anisotropic properties observed in sculptured films produced by GLAD technique are attributed to the columnar structure of the films. Because of morphology-manipulating capability of GLAD technique, optically isotropic materials can be engineered into anisotropic forms. The GLAD films made of naturally isotropic materials can exhibit large anisotropy. However, natural anisotropic materials often cannot be fabricated as thin films [16]. The limited number of natural birefringent compounds is an obstacle for developing optical devices [17]. Thus, the GLAD technique may provide a route to obtain greater optical birefringence [16]. The degree of this anisotropy strongly depends on the kind of material and the deposition conditions such as deposition angle [7,13]. The anisotropic magnitude and orientation can be varied through changing the thickness of the film via deposition angle adjustment, which is an important feature of GLAD technique used to fabricate polarization discriminating optics [18].

Thin films possessing optical anisotropy exhibit various applications such as optical retardation plates [19], anisotropic antireflection coatings [20], birefringent omnidirectional reflectors [21], three-dimensional photonic bandgap crystals [22], birefringent thin film polarizers [23], novel optical filters [14], polarization-selective mirrors and interference filters [24].

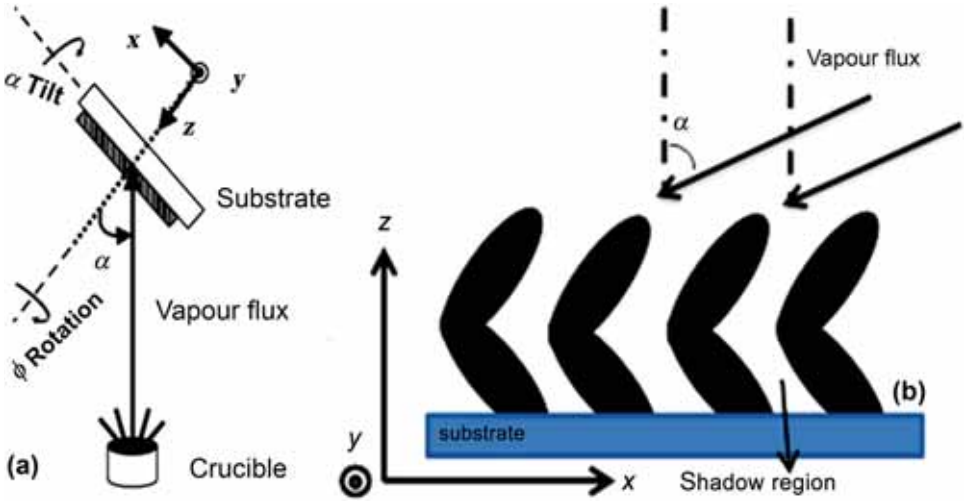


**Figure 1.** (**a**) Schematic diagram of the GLAD technique, and (**b**) zigzag pattern formed on the substrate. $x$- and $y$-axes of the coordinate system refer to p- and s-polarization directions, respectively.

So far, the optical anisotropy and in-plane birefringence have been investigated by several groups for slanted post $ZrO_2$ [25], ZnO [26], $Ta_2O_5$ [27], $TiO_2$ [28], $WO_3$ [29] and $Nb_2O_5$ [30] thin films. Also, Wang *et al* [16] discussed the in-plane birefringence of ZnS slanted post films, and obtained the maximum birefringence ($\Delta n = 0.036$) at incident flux angle of $\alpha = 80°$.

However, to the best knowledge of the authors, the anisotropic optical properties of ZnS zigzag films have not been reported so far. Thus, the present study may help one to understand the relation between the deposition parameters of a GLAD ZnS zigzag structure and its anisotropic optical properties.

The present work is the extension of our investigation on structural and optical properties of ZnS zigzag nanostructured thin films [31]. Here, the effect of different deposition angles ($\alpha = 0$, 30, 60, 70 and 80°) on the optical and the structural anisotropic properties of ZnS zigzag thin films fabricated using GLAD technique is reported. The s- and p-refractive indices, the porosity and the in-plane birefringence at various deposition angles are evaluated.

## 2. Experimental

ZnS zigzag nanostructured layers have been grown on to glass substrates by thermal evaporation method in a Hind-HIVAC coating unit (Model ISF6) equipped with a GLAD system [31]. Two stepper motors along with an Alf-Egil Bogen, Vegard Wollan, RISC (aka Advanced Virtual RISC) AVR microcontroller were introduced into the vacuum system to tilt and rotate the substrate automatically, as shown in figure 1a. The incident flux angle ($\alpha$) was measured as the direction of the incident flux with respect to the substrate normal. The substrates were cleaned in acetone using an ultrasonic bath and then dried by purified nitrogen gas. Initial pressure of the chamber was about $10^{-6}$ mbar. A ZnS tablet of 99.99% purity, supplied by Aldrich Company, was evaporated from a molybdenum boat. The deposition rate and the thickness of film were measured and controlled *in-situ* using a Hind-HIVAC thickness monitor (Model DTM-101). The average deposition rate was 5 Å $s^{-1}$. In order to achieve a uniform layer on the substrate, the distance between the evaporation source and the substrate was 30 cm. During the deposition process, the substrate was kept at room temperature by means of a circulating cold water system including a copper block acting as a heat exchanger attached to the sample holder [32].

For fabrication of the zigzag structure (figure 1b), the first branch was deposited on the substrate at a given $\alpha$ value. In order to produce the second branch, the substrate was rotated by 180° about its normal axis (angle $\phi$) without opening the vacuum chamber.

In this experiment, five ZnS films were prepared with the same nominal branch thicknesses at various incident flow angles of 0, 30, 60, 70 and 80°, which were labelled, respectively, as Z0, Z30, Z60, Z70 and Z80.

The prepared samples were systemically studied by the following techniques. X-ray diffraction (XRD) used in the present study is through a D8-Advance Bruker instrument equipped with a Cu-$k_\alpha$ radiation source with $\lambda$ = 1.5406 Å, acceleration voltage of 40 kV and electron current of 40 mA, which is configured in horizontal theta–2theta ($\theta$–$2\theta$) geometry. The UV–VIS spectrophotometer employed in the present investigation is a Lambda 900 Perkin-Elmer equipment. The transmittance spectra were measured in terms of wavelength, in the wavelength range 350–850 nm. The polarized test lights (s and p) used in this measurement were impinged on the substrate surface at two different angles, $\theta = 0$ and 70°.

## 3. Results and discussion

### 3.1 *Structural analyses*

Figure 2 presents the XRD patterns of thermally evaporated ZnS films grown at different incident flow angles, 0, 30, 60, 70 and 80°. Three peaks at $2\theta \approx 29$, 48 and 57° are observed in all the XRD spectra. These diffraction angles belong to cubic crystal (111), (200) and (311) planes, correspondingly, with (111) plane as the preferential direction. In general, ZnS films crystallize in both cubic and/or hexagonal structure depending on the deposition technique [33]. Recently, Yin *et al* [34] and Hichou *et al* [35] reported cubic and a mixture of cubic and hexagonal phases for ZnS films prepared by homogeneous precipitation at different pH values and spray pyrolysis techniques, respectively.

As mentioned earlier, all the samples were found to be cubic in structure with F-43m space group, which is quite predictable since in this work the deposition was made on substrates maintained at room temperature. A similar effect of substrate temperature on the crystallographic phase of ZnS films has been reported by other authors [36,37].

Figure 2b clearly shows that intensity and width of diffraction peaks of the grown films decrease upon increasing incidence angle, which are characteristics of the GLAD technique. Reduction of the width of diffraction peak indicates the crystallite size increment of the samples, which has been attributed to the shadowing effect by Vick *et al* [6]. It has been shown that when a flux of the atomic vapour comes at a given angle (say $\alpha$), deposition rate will have a lateral as well as a vertical component with respect to the substrate surface. The lateral component helps the nucleation sites intercept the incident particles and causes the shadowing effect to happen. During this process, a growth competition occurs among the columns, which lets the tallest nucleated islands to keep growing by receiving more atoms than the shorter ones. Eventually, a tilted columnar film with an angle different from $\alpha$ (say $\beta$) is formed [6,7].

It is also observed from figure 2b that a gradual decrease in the main peak intensity occurs upon increasing the incident flow angle. This is one of the features of GLAD technique that has been frequently reported [16,25,38].

The average grain size ($D$) for ZnS films is calculated from the width of (111) peak at half maximum intensity ($\kappa$) using the Debye–Scherrer formula [33] given by the relation

$$D = \frac{0.9\lambda}{\kappa \cos\theta}, \tag{1}$$

where $\theta$ is the diffraction angle and $\lambda$ is the X-ray wavelength (1.5406 Å).

The inter-planar spacing ($d$) is evaluated using the standard Bragg's relation

$$d = \frac{n\lambda}{2\sin\theta}. \tag{2}$$

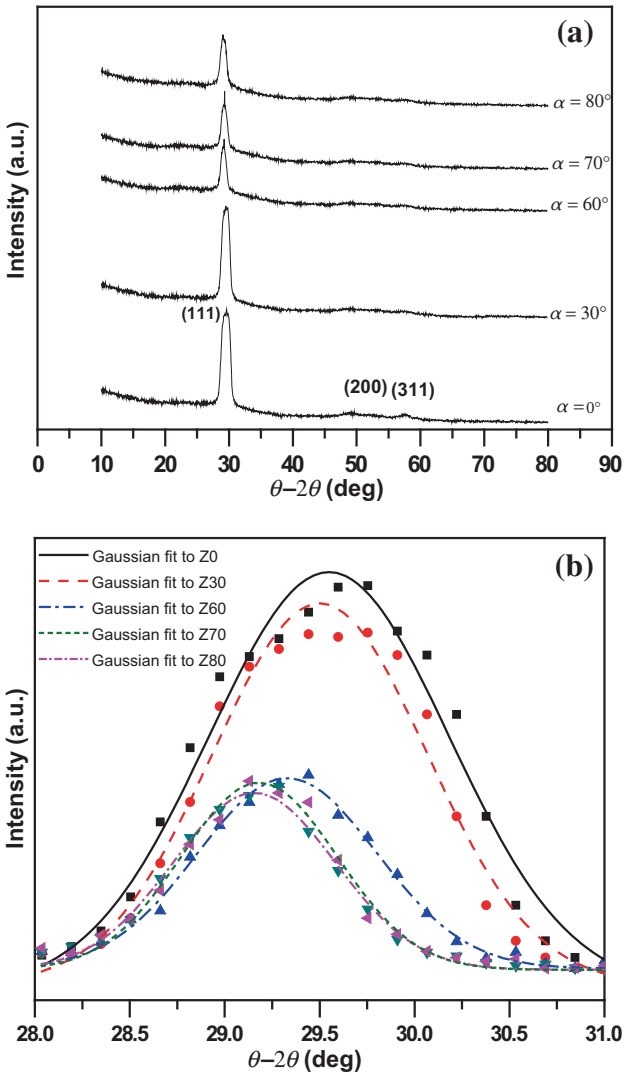


**Figure 2.** (**a**) XRD patterns of ZnS films under different conditions and (**b**) Gaussian fitting for the main peak.

The lattice constant ($a$) for the cubic phase of ZnS film is determined using the following equation [33]:

$$a = d\left(h^2 + k^2 + l^2\right)^{0.5}, \tag{3}$$

where $h$, $k$ and $l$ denote the Miller indices of the lattice planes.

The measured lattice parameter of ZnS film deviates from that of bulk ZnS and this is supposed to be the cause of intrinsic stress ($\sigma_s$) developed in the film. It is calculated using the following relation [39]:

$$\sigma_s = \frac{Y(a - a_0)}{2a_0\gamma}, \tag{4}$$

where '$Y$' is Young's modulus of ZnS (75 GPa), '$a$' is the lattice constant measured from the XRD data, '$a_0$' is the bulk lattice constant (5.406 Å) and '$\gamma$' is Poisson's ratio (0.28) for

**Table 1.** Structrual data of the zigzag ZnS films calculated from XRD analysis for (111) plane.

| Film | $2\theta$ (°) | $\beta$ (°) | $k$ (°) | $d$ (Å) | $D$ (Å) | $a$ (Å) | $\sigma_s$ (GPa) | $\delta$ ($\times 10^{-4}$) (Å$^{-2}$) |
|---|---|---|---|---|---|---|---|---|
| Z0 | 29.550 | 1.51 | 1.51 | 3.020 | 55.18 | 5.231 | −4.340 | 3.264 |
| Z30 | 29.501 | 1.33 | 1.33 | 3.025 | 61.72 | 5.240 | −4.125 | 2.604 |
| Z60 | 29.329 | 1.11 | 1.11 | 3.043 | 73.91 | 5.271 | −3.354 | 1.805 |
| Z70 | 29.155 | 1.01 | 1.01 | 3.060 | 81.60 | 5.300 | −2.623 | 1.473 |
| Z80 | 29.121 | 0.97 | 0.97 | 3.064 | 84.88 | 5.307 | −2.452 | 1.361 |

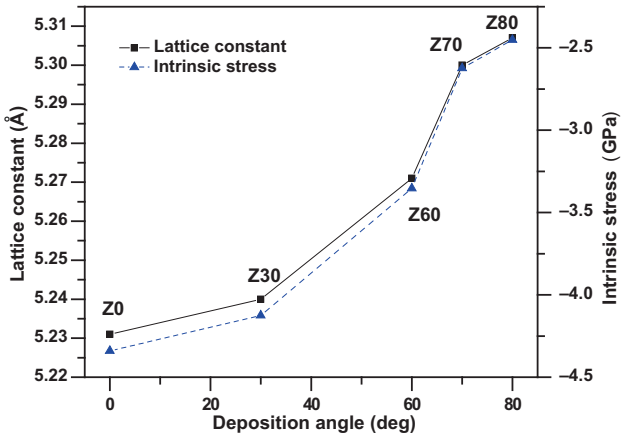


**Figure 3.** Variation of lattice constant and intrinsic stress *vs.* incident flow angles for all samples.

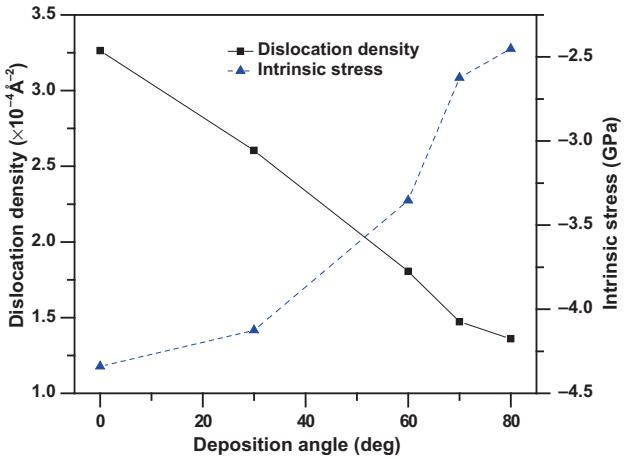


**Figure 4.** Dislocation density and intrinsic stress *vs.* deposition angles for all samples.

ZnS [33]. If $a > a_0$, the stress is of tensile type, whereas, if $a < a_0$, it is of compressional type.

The following relation was used to determine the dislocation density ($\delta$) [40]:

$$\delta = \frac{15\kappa \cos\theta}{4aD}. \tag{5}$$

The structural parameters such as inter-planar spacing, lattice constant, crystallite size, intrinsic stress and dislocation density were calculated using these equations and are given in table 1.

From XRD patterns and table 1, the position of the main peak is found to move slightly towards lower diffraction angles, which may be attributed to the stress developed in films caused by formation of zigzag structure. The variations of lattice constant and intrinsic stress, and tensile stress and dislocation density for ZnS films *vs.* deposition angle are shown in figures 3 and 4, respectively.

It can be seen from figure 3 that the lattice constant values slightly increase with increment of incidence angle. These values are smaller than the bulk lattice constant of ZnS. This increase of lattice constant towards the bulk value corresponds to decreasing intrinsic stress, which is in accordance with Eq. (4). The intrinsic stress indicates the presence of compressional strain in the samples, which comes down and approaches the tensile strain. It is well known that higher the vapour flux angle ($\alpha$), lower the thickness of the deposited film. Therefore, this reduction in compressional strain may be attributed to the dependence of zigzag thin film thickness on incident flow angle. Other deposition parameters may have similar effects on compressional strain. For example, Ennos [41] reported the compressional stress developed in ZnS films that decreased with increasing substrate temperature.

During initial growth, as the incidence angle $\alpha$ increases, the formed islands start collecting more ad-atoms. They will grow faster and tend to capture more incoming vapour flux, reinforcing the growth of large crystallites at the expense of other grains that are consumed during the process [29]. This possible interpretation of the long-range crystalline ordering agrees well with the increment of the crystallite size obtained from the XRD measurements (see table 1).

Figure 4 illustrates the variation of dislocation density and intrinsic stress in terms of deposition angle for all the samples. Decrement of dislocation density with increment of incident flow angle is observed, which may be due to reduction of internal stress upon increasing deposition angle. It is also seen that a rapid increment in the dislocation density initially happens up to 70°, followed by lower rate of decrement. It is observed

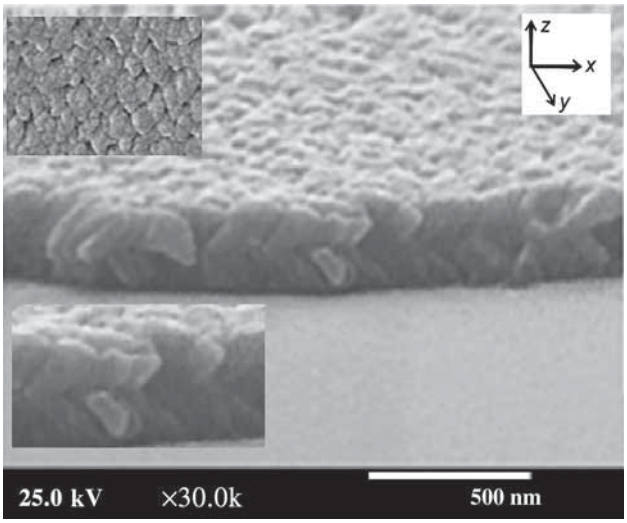


**Figure 5.** Typical cross-sectional and top view FESEM micrograph of ZnS zigzag film $\alpha = 80°$.

from figure 4 that the intrinsic stress decreases with rise of growth angle. This figure also shows that the defects density is inversely dependent on the incident flow angle; hence, one can expect the lattice constants of the samples to become comparable with those of ZnS bulk materials as the incidence angle is increased.

### 3.2 *Microstructure of the GLAD films*

Figure 5 shows typical cross-sectional and top view FESEM micrographs of ZnS film prepared at $\alpha = 80°$. The figure clearly reveals the formation of zigzag structure of the deposited film. The self-shadowing effect and limited adatom mobility during the oblique deposition can be the reason for the formation of ZnS microstructures. The cross-sectional view of the sample shows that the GLAD ZnS film is composed of slanted columns and inter-columnar gaps (voids spacing) with columns showing inclination towards the direction of the incoming vapour. The same behaviour has been reported by Charles *et al* [29] in the case of $WO_3$ thin film growth by GLAD technique.

Based on previously reported results [31], the inter-columnar gaps increase with the increment of flux angle. At higher flux angles (e.g., 80°), the shadowing effect dominates the limited ad-atom mobility and hence films morphology changes and the columns become increasingly separated and distinguishable; thus, porous and highly orientated microstructures composed of slanted columns are produced. The cross-sectional morphology agrees well with the zone 1 structure of well-known Thornton's structural zone model [42,43], which is due to the limited mobility of the incoming atoms during the oblique deposition process [44].

The highly orientated slanted columns indicate that GLAD ZnS films are anisotropic with the long axis parallel to the columnar growth direction [45]. Brian and Michael [46] have stated that the anisotropic structure will introduce the anisotropic dependence on the thermal, electrical, magnetic and optical properties of thin films. At $\alpha = 80°$, the film surface porosity was found to increase significantly [31]. It is also seen that the porosity of film's surface is asymmetric in the $x$- and the $y$-directions and the film is more porous in the $x$-direction. The same kind of structural anisotropy was reported in the case of obliquely deposited ZnS thin film by Tait *et al* [47]. It is observed from figure 5 that the columns are almost in intimate contact with each other along $y$-axis while they are not so along $x$-axis.

### 3.3 *Optical properties of the GLAD films*

As mentioned before, the prepared films are anisotropic. This property is expected to affect the optical properties of these samples; hence the measurement of the optical parameters would be of great interest. Recently, Lakhtakia and Messier [22], in their book about STFs, have provided a basic knowledge of the morphology and the optical response characteristic of STFs. They have simulated and shown that the transmittance of such films highly depends on light polarization and incident light angle ($\theta$). Thus, in the present investigation, optical s- and p-polarized transmittance spectra of the prepared specimens were obtained in the visible range and they are presented in figure 6a–c.

In figure 6, $T_s$ and $T_p$ represent the s- and p-polarized transmittance spectra for all samples, respectively. The polarized test lights (s and p) arriving at the substrate surface at two different angles, 0 and 70°, were used to study the effect of incident light angle on the optical constants of the samples. As expected, typical interference fringes are observed in the transmittance spectra of the films. The oscillation frequency depends on the refractive index and film thickness. The film deposited by conventional process ($\alpha = 0°$) exhibits the lowest transmission amplitude. The transmittance of the samples clearly increases with increment of deposition angle. The same behaviour has been observed by other authors [48–50].

From the inset of figure 6b, showing $T_s$ and $T_p$ curves for sample Z60, one can clearly see that the s- and p-polarization spectra at normal incidence light are almost the same. This is because the electric field component of normal incidence light ($\theta = 0°$) for both the polarizations lie on the film surface.

Considering figure 6a–c, it can be found that one of the important factors that affect the transmission behaviour of STFs is the incident light angle. At normal incidence angle, the difference between s- and p-polarization spectra is almost insignificant (figure 6a and b), while this difference becomes more distinguishable at higher incident light angles (figure 6c). It is clearly observed from figure 6c that the variation behaviour of s-polarized light with the incident light angle is not as periodic as it is in the case of p-polarized light. In addition, the percentage of $T_p$ is much higher than that of $T_s$.

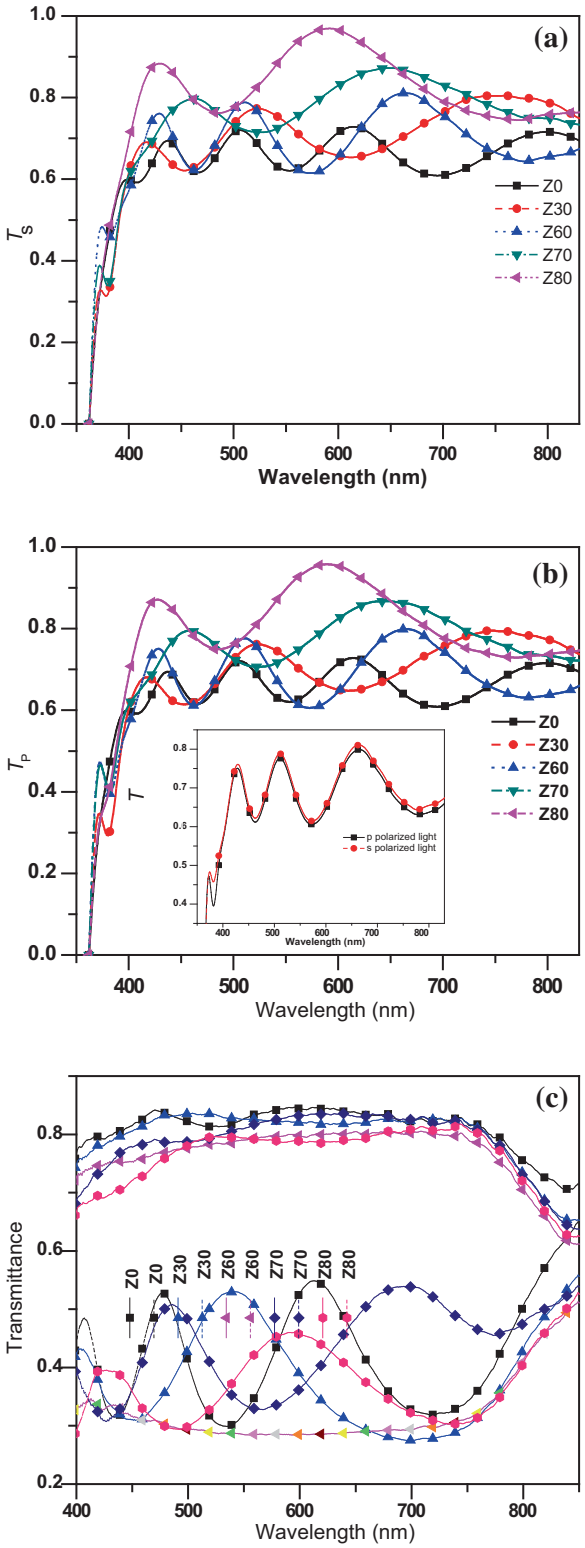


**Figure 6.** Wavelength dependence of (**a**) s-polarization transmission spectrum at normal light incidence angle for all samples. (**b**) p-polarization transmission spectrum at normal light incidence angle for all samples, the inset exhibits the $T_s$ and $T_p$ for sample Z60. (**c**) s- and p-polarization transmission spectrum at 70° light incidence angle for all samples.

This difference is due to the incident light angle approaching the Brewster angle [51,52], which is equal to 67.38° for the bulk ZnS material at wavelength of 600 nm [53]. It is well known that at an incident light angle near the Brewster angle, the reflectance of p-polarized light is very close to zero. It is worth noting that the Brewster angle for thin film of a material is different from that of its bulk. It should also be noted that the same difference in nature of periodic behaviour and magnitudes of the s- and p-polarization spectra at higher incident light angles, especially when approaching the Brewster angle, has been predicted theoretically by Siabi-Garjan *et al* [54]. The knowledge on optical constants of thin films is extremely important in determining their usage in the applications such as wave-guiding devices, photoelectric behaviour and analysis of heterostructure layers [33].

In the present study, the envelope method proposed by Swanepoel [55] was applied for the determination of optical parameters using interference fringes in optical transmittance spectra. It is known that the transmittance ($T$) of a thin film is a function of refractive index ($n$), absorption coefficient ($\alpha$) and wavelength ($\lambda$) given by

$$T = \frac{Ax}{B - Cx\cos\varphi + Dx^2},$$
$$A = 16sn^2,\ B = (n+1)^3\left(n+s^2\right),$$
$$C = 2\left(n^2-1\right)\left(n^2-s^2\right),\qquad D = (n-1)^3\left(n-s^2\right),$$
$$\varphi = \frac{4\pi nh}{\lambda},\qquad \alpha = \frac{-\ln(x)}{h}. \tag{6}$$

Here, $s$ is the refractive index of substrate and $h$ is the film thickness. The refractive index of film is given by

$$n(\lambda) = \left[N^{1/2} + \left(N^2 - s^2\right)^{1/2}\right]^{1/2}, \tag{7}$$

$$N = 2s\left(\frac{T_{\max} - T_{\min}}{T_{\max}T_{\min}}\right) + \frac{s^2+1}{2}. \tag{8}$$

Here, $T_{\max}$ and $T_{\min}$ are the maximum and minimum of the interference fringes in transmittance values on the envelope drawn over the interference peaks in the spectrum.

It is well known from linear optics that when transmittance spectra ($T_s$ and $T_p$) are obtained at two orthogonal directions of incident linear polarized light directions ($x$ and $y$ directions axes shown in figure 1b), then in-plane birefringence can be defined as the difference ($n_p - n_s$) between two in-plane refractive indices [17]. Here, $n_s$ and $n_p$ are determined by the Swanepoel method from $T_s$ and $T_p$ transmission curves (shown in figure 6a and b), respectively, and the results have been demonstrated in figure 7.

The refractive index curves of ZnS films deposited at various incidence angles are fitted using the Cauchy dispersion equation

$$n(\lambda) = A_1 + A_2/\lambda^2 + A_3/\lambda^4. \tag{9}$$

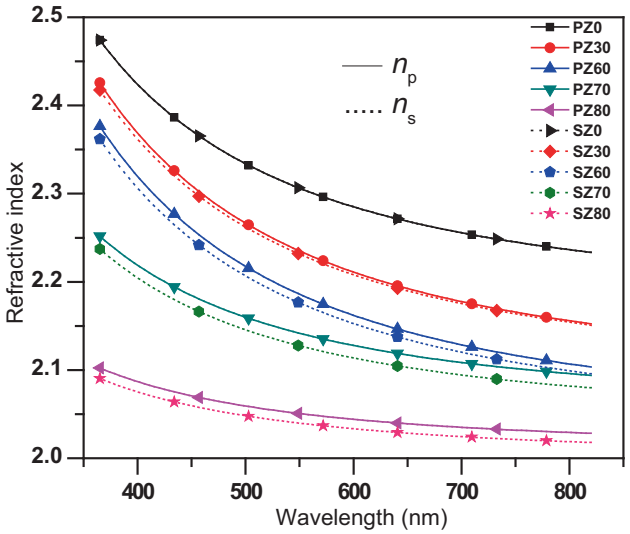


**Figure 7.** Fitted dispersion curves of s- and p-refractive indices of ZnS zigzag thin films with different incidence angles.

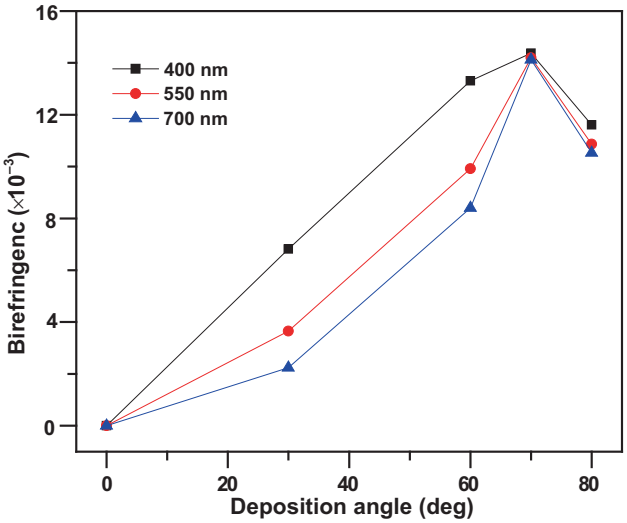


**Figure 8.** Calculated in-plane birefringenece of GLAD ZnS films at selected wavelength.

It is observed from figure 7 that ZnS thin film prepared at normal incidence flow angle (Z0) exhibits the highest refractive index. It may be noted that at $\alpha = 0$, both the $n_s$ and $n_p$ values are the same in the entire wavelength range of study. For a given wavelength, say 550 nm, $n_s$ and $n_p$ values are equal to 2.30, which is less than the refractive index of ZnS bulk material (2.39) [53]. This difference may be attributed to the presence of porosity in the deposited films. This figure also shows that the refractive indices of GLAD ZnS films are $n_p = 2.14$ and $n_s = 2.12$ for Z70, and $n_p = 2.05$ and $n_s = 2.03$ for Z80 at $\lambda = 550$ nm.

Figure 8 illustrates the curves corresponding to in-plane birefringence $\Delta n$ for all specimens at 400, 550 and 700 nm. These curves show a similar behaviour; that is, at $\alpha = 0$, all the samples show no birefringence but as the incidence angle is increased, the samples show birefringence $\Delta n$, which reaches its highest value at $\alpha = 70°$. As the deposition angle is increased beyond 70°, birefringence decreases, which indicates reduction of optical anisotropic properties of films. It is interesting to note that the same behaviour in the case of GLAD-deposited $ZrO_2$ [25], ZnS [16], $WO_3$ [29], $Ta_2O_5$ [27] and $TiO_2$ [28] films have been reported. It is also seen from figure 8 that for a given deposition angle, $\Delta n$ value is higher for lower wavelength. This may be due to the fact that when the incident light wavelength becomes higher than the layer thickness, $\Delta n$ value decreases. A maximum birefringence value equal to 0.014 was obtained with an oblique angle of $\alpha = 70°$, which is higher than that of the common anisotropic bulk materials such as quartz ($\Delta n = 0.009$) and $MgF_2$ ($\Delta n = 0.012$) at 633 nm wavelength [17]. However, the obtained value for $\Delta n$, that is 0.014, is less than the value reported by Wang *et al* [16] for the ZnS film with tilted structure ($\Delta n = 0.034$). The fact that $\Delta n$, in the case of zigzag structure, is less than that in the tilted structure has been also reported by Woo and Hwangbo [28] in the case of $TiO_2$ films. They found $\Delta n$ for tilted, zigzag and helical $TiO_2$ films equal to 0.063, 0.053 and 0.004 at 633 nm wavelength, respectively. They attributed this finding to the symmetric incoming vapour flux.

Therefore, it can be deduced that the GLAD technique is a promising one to produce films with anisotropic behaviour. The anisotropic properties of the GLAD films are related to the biaxial columnar structures reported by Charles *et al* [29].

The Bruggeman effective-medium approximation is given by [56]

$$P_m \frac{\varepsilon_m - \varepsilon}{\varepsilon_m + 2\varepsilon} + P_v \frac{\varepsilon_v - \varepsilon}{\varepsilon_v + 2\varepsilon} = 0, \tag{10}$$

where $P_m$ and $P_v$ $(1 - P_m)$ are the packing density of material and the porosity or packing density of void, respectively; $\varepsilon$, $\varepsilon_m$ and $\varepsilon_v$ are the dielectric functions of the effective medium, material and void, respectively. In the low light absorption region, $n^2 >> k^2$ and $\varepsilon = n^2$ (refractive index of films), $\varepsilon_m = n_m^2$ (refractive index of bulk ZnS) and $\varepsilon_v = n_{air}^2$ (refractive index of air).

Table 2 presents the calculated $P_m$ and $P_v$ values for the samples prepared at different incident flow angles. Using the data presented in this table, figure 9 has been drawn to show the variation of packing density and p-refractive index with incidence angle for GLAD ZnS thin films. From table 2, it is clear that the packing density of the samples decreases on increasing the deposition angle. At incidence angle $\alpha = 80°$, the packing density falls to 0.797, which means that the specimen prepared at the highest incidence angle is more porous than the others. Prathap *et al* [57] also reported a similar dependence of packing density on $\alpha$ value in deposition of ZnS films by close-spaced thermal evaporation ZnS films.

**Table 2.** The packing density and effective refractive indices of the samples for p- and s-polarization.

| | Refractive index at $\lambda = 550$ nm | | Packing density | | Porosity (%) | |
|---|---|---|---|---|---|---|
| Samples | $n_p$ | $n_s$ | p | s | p | s |
| Z0 | 2.306 | 2.306 | 0.9510 | 0.9510 | 4.902 | 4.902 |
| Z30 | 2.235 | 2.232 | 0.9090 | 0.907 | 9.097 | 9.276 |
| Z60 | 2.187 | 2.178 | 0.8804 | 0.8750 | 11.962 | 12.502 |
| Z70 | 2.142 | 2.128 | 0.853 | 0.845 | 14.671 | 15.519 |
| Z80 | 2.050 | 2.040 | 0.797 | 0.791 | 20.284 | 20.901 |

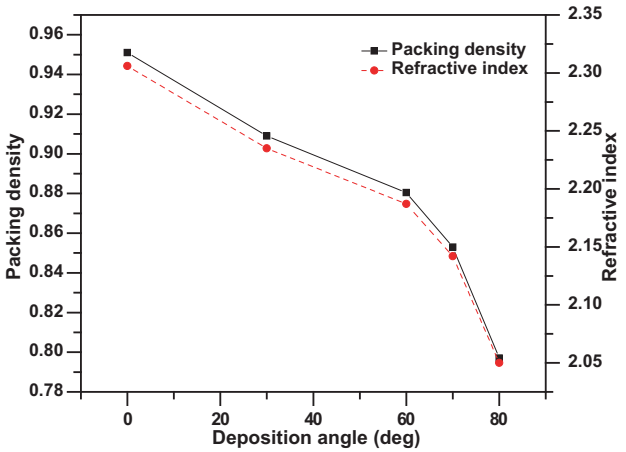


**Figure 9.** Refractive index and packing density as functions of deposition angle for p-polarization for all samples.

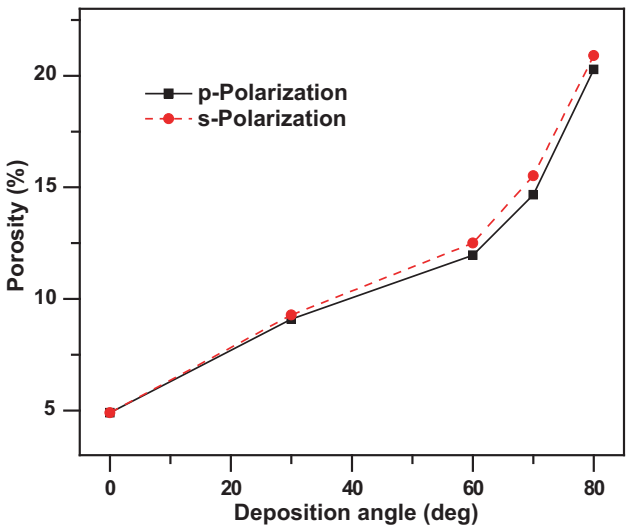


**Figure 10.** Comparison of the porosity variation of ZnS films for both polarization directions with deposition angle at incident light wavelength of 550 nm.

Figure 10 demonstrates the variation in porosity of the samples in $x$- and $y$-directions as a function of deposition angle. It is seen in this figure that the porosity in the $y$-direction (perpendicular deposition plane) is higher than that in $x$-direction and the difference between porosity in these two directions increases with increasing deposition angle up to 70°, which then decreases with further increase of $\alpha$ value.

It is well known that porosity of a film produced by GLAD technique is a consequence of shadowing effect during the deposition process. The shadowing effect is always stronger in deposition plane compared with its perpendicular plane, which leads to the formation of columns more separated from each other in the former plane than in the latter. This leads to structural anisotropic properties of the films. Abelmann and Lodder [58] introduced another type of anisotropy considering the cross-sectional shape of the columns.

As is well known, the column cross-sections are generally elliptical in shape, with the long axis of ellipse either parallel or perpendicular to the vapour incidence plane [58]. Considering the arrival of vapour atoms at the substrate surface obliquely, islands are formed on the surface connecting to each other perpendicular to the shadowing direction. Hence, the shadowing effect is the cause of structural anisotropy developing parallel to the substrate surface.

In the present study, it is found that as the incidence angle approaches 70°, the shadowing effect dominates the surface diffusion. Increasing the $\alpha$ value beyond 70° will lead to decrease of islands concentration on the surface since the shadowing effect becomes more effective. Therefore, column tapering will cause an islands separation increment. Charles *et al* [29] have interpreted these phenomena as the reason for loss of anisotropy.

## 4. Conclusion

ZnS STFs were prepared by thermal evaporation method using GLAD technique. XRD analysis revealed cubic structure of the prepared samples. Optical studies of the deposited films showed that the refractive index of the GLAD films is less than that of ZnS bulk material. Optical birefringence at visible and near infrared wavelengths was found to vary with incidence angle, with the maximum $\Delta n = 0.014$ at $\alpha = 70°$. This calculated maximum value of $\Delta n$ for zigzag structure

is less than that for slanted structure due to lower porosity associated with zigzag structure. The s- and p-polarization transmission spectra of the samples for the polarized test light angle of 70° were found to have significant difference, indicating that the employed angle was above the Brewster angle of ZnS film.

## References


[1] Young N and Kowal I 1959 *Nature (London)* **183** 104
[2] Robbie K, Beydaghyan G, Brown T, Dean C, Adams J and Buzea C 2004 *Rev. Sci. Instrum.* **75** 1089
[3] Barranco A, Borras A, Gonzalez-Elipe A R and Palmero A 2016 *Prog. Mater. Sci.* **76** 59
[4] Siyanaki F H, Dizaji H R, Ehsani M H and Khorramabadi S 2015 *Thin Solid Films* **577** 128
[5] Vick D, Smy T and Brett M J 2002 *J. Mater. Res.* **17** 2904
[6] Vick D, Friedrich L J, Dew S K, Brett M J, Robbie K, Seto M *et al* 1999 *Thin Solid Films* **339** 88
[7] Robbie K 1998 PhD Thesis (Alberta: University of Alberta)
[8] Gonzalez-Garcia L, Parra-Barranco J, Sanchez-Valencia J R, Barranco A, Borras A and Gonzalez-Elipe A R 2012 *Nanotechnol.* **23** 205701
[9] Dick B, Brett M J and Smy T 2003 *J. Vac. Sci. Technol. B* **21** 23
[10] Abdi F and Savaloni H 2015 *Appl. Surf. Sci.* **330** 74
[11] Lintymer J, Martin N, Chappe J M, Delobelle P and Takadoum J 2004 *Surf. Coat. Technol.* **26** 180
[12] Holland L 1953 *J. Opt. Soc. Am.* **43** 376
[13] Woo S-H and Hwangbo C K 2006 *J. Korean Phys. Soc.* **48** 1199
[14] Hodgkinson I J and Wilson P W 1988 *CRC Crit. Rev. Solid State Mater. Sci.* **15** 27
[15] Kranenburg H van, Lodder J C, Maeda Y, Toth L and Pompa J A 1990 *IEEE Trans. Magn.* **26** 1620
[16] Wang S, Fu X, Xia G, Wang J, Shao J and Fan Z 2006 *Appl. Surf. Sci.* **252** 8734
[17] Beydaghyan G, Kaminska K, Brown T and Robbie K 2004 *Appl. Opt.* **43** 5343
[18] Martin P M 2009 *Handbook of deposition technologies for films and coatings: science, applications and technology,* 3rd edn (Holland: Elsevier)
[19] Motohiro T and Taga Y 1989 *Appl. Opt*. **28** 2466
[20] Xi J Q, Schubert M F, Kim J K, Schubert E F, Chen M F, Lin S Y *et al* 2007 *Nat. Photon.* **1** 176
[21] Kaminska K and Robbie K 2004 *Appl. Opt.* **43** 1570
[22] Lakhtakia A and Messier R 2005 *Sculptured thin films—nanoengineered morphology and optics* (Bellingham, WA: SPIE)
[23] Hodgkinson I J and Wu Q H 1999 *Appl. Phys. Lett.* **74** 1794
[24] McPhun A J, Wu Q H and Hodgkinson I J 1998 *Electron. Lett.* **34** 360
[25] Sobahan K M A, Park Y J and Hwangbo C K 2010 *J. Korean Phys. Soc.* **56** 1282
[26] Park Y J, Sobahan K M A, Nam H J, Kim J J and Hwangbo C K 2010 *J. Korean Phys. Soc*. **57** 1657
[27] Hodgkinson I J and Wu Q H 1999 *Appl. Opt.* **38** 3621
[28] Woo S H and Hwangbo K 2006 *J. Korean Phys. Soc.* **49** 2136
[29] Charles C, Martin N, Devel M, Ollitrault J and Billard A 2013 *Thin Solid Films* **534** 275
[30] Xiao X, Dong G, Xu C, He H, Qi H, Fan Z *et al* 2008 *Appl. Surf. Sci.* **255** 2192
[31] Rahchamani S Z, Dizaji H R and Ehsani M H 2015 *Appl. Surf. Sci.* **356** 1096
[32] Rahchamani S Z, Dizaji H R and Ehsani M H 2015 *Procedia Mater. Sci.* **11** 464
[33] Subbaiah Y P V, Prathap P and Reddy K T R 2006 *Appl. Surf. Sci.* **253** 2409
[34] Yin L, Zhang D, Wang D, Kong X, Huang J, Wang F *et al* 2016 *Mater. Sci. Eng. B* **208** 15
[35] Hichou A E, Addou M, Bubendorff J L, Ebothe J, Idrissi B E and Troyon M 2004 *Semicond. Sci. Technol.* **19** 230
[36] Chelvanathan P, Yusoff Y, Haque F, Akhtaruzzaman M, Alam M M, Alothman Z A *et al* 2015 *Appl. Surf. Sci.* **334** 138
[37] Jin C, Kim H, Park S, An S and Lee C 2013 *Phys. Scr. T* **157** 014043
[38] Leem J W and Yu J S 2011 *Opt. Express* **19** 258
[39] Chopra K L 1969 *Thin film phenomena* (New York: McGraw–Hill) p 270
[40] Warren B E 1969 *X-ray diffraction* (London: Addison Wiley Publishing Co.) p 18
[41] Ennos A E 1966 *Appl. Opt.* **5** 51
[42] Movchan B A and Demchishin A V 1969 *Phys. Met. Metallogr.* **28** 83
[43] Thornton J A 1977 *Ann. Rev. Mater. Sci.* **7** 239
[44] Levichkova M, Mankov V, Mednikarov B and Starbova K 2001 *Surf. Coat. Technol.* **141** 70
[45] Kranenburg V H and Lodder C 1994 *Mater. Sci. Eng. R* **11** 295
[46] Brian D and Michael B J 2004 *Encyclopedia Nanosci. Nanotechnol.* **6** 703
[47] Tait R N, Smy T and Brett M J 1992 *J. Vac. Sci. Technol. A* **10** 1518
[48] Ehsani M H, Dizaji H R, Azizi S, Mirmahalle S F G and Siyanaki F H 2013 *Phys. Scr.* **88** 025602
[49] Kim D, Park Y, Kim M, Choi Y, Park Y S and Lee J 2015 *Mater. Res. Bull.* **69** 78
[50] Deshmukh H P, Shinde P S and Patil P S 2006 *Mater. Sci. Eng. B* **130** 220
[51] Jackson J D 1975 *Classical electrodynamics*, 2nd edn (New York: Wiley)
[52] Reitz J R and Milford F J 1960 *Foundations of electromagnetic theory* (Reading, MA: Addison-Wesley)
[53] Palik E D 1985 *Handbook of optical constants of solids* (New York: Academic)
[54] Siabi-Garjan A, Savaloni H, Abdi F, Ghaffal A and Placido F 2013 *Phys. Scr.* **87** 055705
[55] Swanepoel R 1983 *J. Phys. E: Sci. Instrum.* **16** 1214
[56] Stroud D 1998 *Superlattices Microstruct.* **23** 567
[57] Prathap P, Revathi N, Subbaiah Y P V and Reddy K T R 2008 *J. Phys.: Condens. Matter* **20** 035205
[58] Abelmann L and Lodder C 1997 *Thin Solid Films* **305** 1